SARS-CoV-2 infection of ocular cells from human adult donor eyes and hESC-derived eye organoids

Bar Makovoz[2,3,#], Rasmus Møller[4,#], Anne Zebitz Eriksen[1,2,3,#], Benjamin R. tenOever[4,*], Timothy A Blenkinsop[1,2,3,*]

[1]Department of Cell Development and Regenerative Biology

[2]Black Family Stem Cell Institute

[3]Department of Ophthalmology

[4]Department of Microbiology

Icahn School of Medicine at Mount Sinai, New York, NY 10029, USA

[#]Co-first author

*Correspondence:

Timothy A Blenkinsop, timothy.blenkinsop@mssm.edu, 1428 Madison Avenue, NY, NY 10029

Benjamin R. tenOever, Benjamin.tenOever@mssm.edu, 1468 Madison Avenue, NY, NY 10029

Keywords: COVID-19; SARS-CoV-2; coronavirus; cornea; eye organoid; stem cells; human eye; ACE2; TMPRSS2; TMPRSS1E; NFkB; Interferon; Furin

Abstract

The outbreak of COVID-19 caused by the SARS-CoV-2 virus has created an unparalleled disruption of global behavior and a significant loss of human lives. To minimize SARS-CoV-2 spread, understanding the mechanisms of infection from all possible viral entry routes is essential. As aerosol transmission is thought to be the primary route of spread, we sought to investigate whether the eyes are potential entry portals for SARS-CoV-2. While virus has been detected in the eye, in order for this mucosal membrane to be a bone fide entry source SARS-CoV-2 would need the capacity to productively infect ocular surface cells. As such, we conducted RNA sequencing in ocular cells isolated from adult human cadaver donor eyes as well as from a pluripotent stem cell-derived whole eye organoid model to evaluate the expression of ACE2 and TMPRSS2, essential proteins that mediate SARS-CoV-2 viral entry. We also infected eye organoids and adult human ocular cells with SARS-CoV-2 and evaluated virus replication and the host response to infection. We found the limbus was most susceptible to infection, whereas the central cornea exhibited only low levels of replication. Transcriptional profiling of the limbus upon SARS-CoV-2 infection, found that while type I or III interferons were not detected in the lung epithelium, a significant inflammatory response was mounted. Together these data suggest that the human eye can be directly infected by SARS-CoV-2 and thus is a route warranting protection.

Introduction

One of the first widely reported deaths by severe acute respiratory syndrome coronavirus-2 (SARS-CoV-2) in early January 2020 originated from an ophthalmologist in Wuhan who reportedly contracted COVID-19 from an asymptomatic glaucoma patient [1]. Coronaviruses (CoVs) are a large family of RNA viruses common amongst vertebrates[2]. Once thought to only be the result of mild upper respiratory infections, the coronavirus family is divided into four subtypes termed alpha, beta, gamma, and delta, of which NK63 and 229E (alpha coronaviruses) and OC43 and HKU1 (beta coronaviruses) are the most common. The emergence of SARS-CoV-1 (beta coronavirus) in 2002 was the first evidence that this family of viruses could elicit more severe disease, infecting >8,000 individuals worldwide with a fatality rate of ~10%. Ten years later another beta coronavirus emerged termed the Middle East respiratory syndrome-related coronavirus (MERS-CoV) that has infected ~2,500 people with a case-fatality rate of >35% since 2012 [3]. While neither SARS-CoV-1 nor MERS-Cov resulted in a pandemic, the recent 2019 emergence of SARS-CoV-2 has already infected over ten million individuals worldwide and killed more than half a million people. As the virus spread from Asia to Europe and beyond, social distancing and stay at home orders were implemented in an effort to slow spread. In addition to this, the use of face masks were also recommended although this still fails to protect the eyes from contacting the virus. In agreement with research on SARS-CoV-1 and MERS-CoV, SARS-CoV-2 RNA has been found the eye[4], although it is unclear whether virus can enter from the ocular tissue or from an internal cellular origin.

All CoVs share a similar structure consisting of four main structural proteins: spike (S), membrane (M), envelope (E), and nucleocapsid (N) [5]. The S attachment protein binds to host receptors to enter into the target cell and gets primed by cleavage using the host cell proteases, allowing the fusion of viral and cellular membranes. SARS-CoV-1 and -2 enter the host cell via binding to the angiotensin-converting-enzyme-2 (ACE2) receptor and is primed by the Transmembrane Serine Protease 2 (TMPRSS2) and, in the case of SARS-CoV-2, proprotein convertase furin all of which are expressed on the ocular surface of cell[6,7].

Animal studies suggest the eye can serve as a site of replication for numerous respiratory infections. Indeed, a study comparing various routes of entry in Rhesus monkeys confirmed the ability to detect virus in the nasolacrimal and pulmonary system upon SARS-CoV-2 infection via the conjunctiva [8]. In addition, feline CoVs (FCoV) infect between 20 and 60% of domestic and wild cats through the oral-fecal route, demonstrating that this family of viruses have a broad tropism for diverse cell types [9]. Moreover, 90% of those checked had FCoV antigens present in the conjunctiva, suggesting ocular secretions were potentially infectious. Two different strains of mouse hepatitis virus, a murine beta coronavirus, were found to infect retinal glial cells, astrocytes, oligodendrocytes and microglia, leading to inflammation and retinal degeneration [10,11]. While, direct evidence of human ocular cells infected by SARS-CoV-2 is still lacking, results from animal studies make a case to evaluate infection in human cells.

In an effort to determine the susceptibility and virus-host interactions of SARS-CoV-2 and the eye, we utilized a whole-eye organoid model from pluripotent stem cells (hESC and hiPSC) that included the retina, retinal pigment epithelium (RPE), ciliary margin, iris, lens and cornea in this organoid [12]. We also examined adult human ocular cells from cadaver donors for comparison. We found cells that express known corneal and corneal endothelium markers also express both ACE2 and TMPRSS2 and upon SARS-CoV-2 infection, they mount an inflammatory response, which suggests that the eye is susceptible to infection by SARS-CoV-2 and a potential entry route for the virus. Future studies will evaluate whether SARS-CoV-2 preferentially targets these ocular cell types over others for entry into the eye. These data not only increase our understanding of SARS-CoV-2 biology but they emphasize other means by which transmission may persist in the population irrespective of wearing masks.

Results

Single-cell RNA sequencing of SEAM eye organoids identifies six corneal cell type clusters

Eye organoids from human pluripotent stem cells enable testing clinically relevant therapeutic candidates on a mass scale. To this end, we evaluated whether eye organoids were a suitable model to study SARS-CoV-2 infection. We performed a modified version of the protocol of differentiation of human pluripotent stem cells into Self-formed Ectodermal Autonomous Multi-zone (SEAM) of ocular cells [12] (Figure 1A). By one month, four zones with distinct borders and cell morphologies are identifiable in the eye organoids, corresponding to different tissues of the eye, including the retinal pigment epithelium (RPE), neural retina, ciliary body, lens and cornea. Zone 3 exhibits known corneal markers, which express E-cadherin, Pax6 and ZO-1 (*TJP1*) (Figure 1B,C). At day 55, the eye organoid cultures were collected and processed for single-cell RNA sequencing, mapped to the human genome using Cell Ranger, and analyzed using unbiased clustering analyses with the Seurat Package in R. Six distinct clusters were given cornea annotation based on differential gene expression analysis, as visualized by uniform manifold approximation and projection (UMAP) and principal component analysis (PCA) (Figure 1D). Shared genes expressed broadly in the SEAM cornea clusters include KRT5, E-Cad and AQP3, all of which are expressed by the cornea (Figure 1E). Cytokeratin *KRT5* is an intermediate filament and marker of corneal tissue [13]. E-cadherin stains for the region in SEAM of presumptive cornea and was broadly found in all of the presumptive corneal subpopulations. *AQP3* encodes a water channel protein and is essential for transporting water across cell membranes in the cornea in response to osmotic gradients [14]. Other cytokeratins strongly expressed across all corneal populations include *KRT5, KRT8, KRT19, KRT13, KRT15, KRT19* [15]. We generated lists of the genes whose log two-fold change (L2FC) expression distinguish between these clusters. The top 20 genes conferring elevated expression for each cluster were displayed by heat-map (Figure 1F). A list of a subset of genes for each cluster is presented to the right of the heat-map. Additional corneal specific genes were also expressed in varying populations including *TJP1, CLU, GJA1 and MUC16*, all essential for corneal organization, regulation of aggregation, moisture and transparency, respectively (Figure

1G). Interestingly *KRT3*, a known marker of central cornea, was noticeably absent; hence we supposed it might arise later in development. Taken together, we concluded the SEAM eye organoids contain cells of a corneal type and are useful for examining processes involved in ocular SARS-CoV-2 infection.

Expression of SARS-Cov-2 related genes in corneal cells

We next asked if known receptors used by SARS-CoV-2 for cell entry were present in corneal cells. UMAP expression analysis of *ACE2* in presumptive corneal populations in the SEAM eye organoids identified a subset of expressing cells (Figure 2A). *ACE2* expression was highest in cluster 3, which was identified by distinct expression of *β–CAT1, SMIM22, LCN2, RARRES1*, and *LRMP*. This group also expressed the overall highest level of *KRT5*. Jensen TISSUES text mining analysis identified functional categories including eye, stratified epithelium, and blood vessel endothelium (Figure 2B). These categories confirm *ACE2* positive cells are of eye origin, and based on markers, may specify the limbus or conjunctiva. Gene ontological analysis similarly identified genes involved in epidermis development and immune system (Figure 2B). Mouse gene atlas results indicated additional epidermal cell types including the cornea (Figure 2B). Therefore, consistent with our previous study [7], a subset of ocular surface ectoderm cells express *ACE2*.

We next examined the expression of *TMPRSS2*, another receptor involved in the angiotensin-renin pathway and associated with coronavirus infection [16]. Similarly to *ACE2*, we found a subset of presumptive corneal cells expressing *TMPRSS2* (Figure 2C), however the number of cells expressing *TMPRSS2* was much less than the number of cells expressing *ACE2*. Interestingly, the same clusters 1 and 3 possess the highest numbers of cells expressing *TMPRSS2* as *ACE2*. Jensen TISSUES text mining analysis identified terms associated with nerve, eye and stratified epithelium (Figure 2D). Mouse gene atlas similarly identified epithelial tissue types (Figure 2D). Gene ontological analysis of *TMPRSS2* positive cells significantly identified with terms including epidermis development, positive regulation of viral entry into host cell, and negative regulation of epithelial proliferation (Figure 2D). As mentioned, corneal cluster 3 possesses the highest number of *ACE2* and *TMPRSS2* positive cells. We

sought to identify additional markers of group 3 which may be relevant for SARS-CoV-2 infection. We found expression of another *TMPRSS* gene of the same family of *TMPRSS2, TMPRSS11E*. We also evaluated the expression of Basigin (*BSG*), hypothesized to be an alternative entry receptor for SARS-CoV-2 [17,18]. *ACE2*, *TMPRSS2, TMPRSS11E* and *BSG* were found in 16, 6, 13, 67 percent of ocular surface ectoderm, respectively (Figure 2E). Additional genes found in cells expressing *ACE2* included *KRT19, KRT15, TMPRSS11E, MUC1, MUC16*, and *IL1RAP*, confirming not only corneal identity but also immune markers (Figure 2F). Interestingly, *TMPRSS11E* possesses a very similar profile to *ACE2* by violin plots. We asked how similar *TMPRSS11E* is to *TMPRSS2*. By BLAST analysis, these two genes share 42% amino acid identity, with some domains sharing 100% identity. We also compared the domains of TMPRSS11E with TMPRSS2. We included another family member, TMPRSS11D, which is exploited by influenza A virus and MERS [19,20]. Interestingly, structure and domains, including active and glycosylation sites seem to be consistent in all three receptors, including the 3' transmembrane domain (Figure S1). TMPRSS11E and TMPRSS11D are particularly similar and TMPRSS2 seems to have a more complex tertiary structure based on disulfide bonds. The crystal structure of TMPRSS11E has been determined and may provide further insight into how viruses take advantage of these receptors [21]. Given that even a trypsin-like protease is capable of replacing *TMPRSS2* for effective proteolytic cleavage leading to infection[22], *TMPRSS11E* may be an alternative partner for SARS-CoV-2 infection in corneal cells and as such, an inhibitor of TMPRSS11E may be an effective prophylactic against SARS-CoV-2 infection.

SARS-CoV-2 infects corneal cells from adult ocular tissues and SEAM eye organoids

Considering *ACE2* and *TMPRSS2* expression in SEAM eye organoids, we evaluated whether SARS-CoV-2 can infect both SEAM-derived corneal tissues and primary corneal cells isolated from adult human cadaver eye donors. Donor cells were digested with collagenase and plated on Synthemax II (Corning)- coated tissue culture treated plastic, then infected with SARS-CoV-2 at a multiplicity of infection (MOI) = 1.0 for 24 hrs. Cells were then lysed and prepared for bulk RNA sequencing.

Sequences were then mapped to the human genome (GRCh37/hg19) and compared to non-infected control cells from adult tissues. Adult human corneal cells from two genetically different donors were infected with similar efficiency by SARS-CoV-2 (Figure 3A). The 3' end of the genome encodes for at least twelve sub-genomic RNAs (sgRNA) that are only expressed once negative-strand synthesis of the viral genome has been initiated and detection of sgRNAs is therefore indicative of active viral replication [23,24]. An increase of read coverage towards the 3' end in both donors suggests that viral replication is taking place (Figure 3A). Relative gene expression was analyzed, and based on differential gene expression we conducted a network analysis of those genes elevated in samples infected with SARS-CoV-2 (log2 fold change > 0.5, adjusted p-value < 0.05) (Figure 3B). Two networks emerged, one primarily involved in cell-cycle and the other consisting of genes involved in inflammation and response to viral infection (Figure 3C). Some of the candidates already associated with coronavirus infection were present, including *NFKBIA*, *NFKBIZ* and *CXCL1*, all indicative of an NFκB-mediated pro-inflammatory cytokine response. When expanding on the direct differentially expressed genes, we find a greater network of associated genes that includes additional genes known to be involved in the anti-viral response (Figure S2). Similar to the adult human corneal samples, infected SEAM eye organoids also exhibited efficient infection by SARS-CoV-2 (Figure 3D). Bulk RNA sequencing of the infected SEAM organoids revealed expression of *ACE2*, *TMPRSS2*, *BSG*, and another infection-associated protein, *FURIN* (Figure 3E) all involved in viral entry, as well as reads mapping to the viral genome. A Furin-like cleavage site has been identified in the spike protein of SARS-CoV-2 which is not present in any other coronavirus[25]. We therefore returned to the sgRNA-seq and can confirm the presence of subpopulation of corneal cells in the eye organoids expressing Furin (Figure S3). Surprisingly, *members of the type I and III interferon families (IFN-I and IFN-III)* were not detected, consistent with our recent observations that SARS-CoV-2 is effective at suppressing these responses in other epithelial cells[26].

Comparison of ocular cell types to SARS-CoV-2 infection

Susceptibility to SARS-CoV-2 infection requires the expression of receptors and proteases that enable viral entry and cleavage, most notably ACE2 and TMPRSS2. In order to evaluate which ocular tissues express ACE2 and whether expression of this entry factor is consistent with increased susceptibility to SARS-CoV-2 infection, we cultured cell types isolated from 6 regions of adult human cadaver donor globes, including cornea, limbus, sclera, iris, RPE and choroid. Cells were infected with an MOI = 1.0 and incubated for 24hrs, then fixed and stained with anti-SARS-CoV-2 Spike protein antibody and ACE2 antibody, counterstained with DAPI to visualize the nucleus. We find SARS-CoV-2 positive staining in cornea, sclera, limbus and RPE, but not in iris or choroid (Figure 4A). Interestingly, this cell-type specific infection is consistent with expression of *ACE2* in the respective tissues (Figure 2 & 4C). To further evaluate viral gene expression, RNA was isolated from these samples and qPCR specifically examining the transcriptional regulatory sequence of sgRNAs. We observed SARS-CoV-2 sgRNA expression in cornea, sclera, limbus iris, RPE, and choroid, with a somewhat variable expression of *ACE2* in corneal samples, which may explain the relatively lower rate of SARS-CoV-2 replication observed in the central cornea (Figure 4B). Viral gene expression in limbal cells is particularly high, as is the expression of *ACE2* and *TMPRSS2* in these tissues (Figure 4C & D). Considering the limbus is the site of corneal and conjunctival stem cells, the association between this function and higher SARS-CoV-2 infection warrants further study. The possibility that SARS-CoV-2 may exploit the proliferative capability of a stem cell niche is intriguing, and supported by our observation from RNA-seq that a cell cycle network was activated in cells infected with SARS-CoV-2. (Figure 3D, Figure S2). Taken together, this data suggests the ocular surface does not only possess the machinery understood to be necessary for SARS-CoV-2 infection, but do indeed become infected by SARS-CoV-2 when exposed. Ongoing studies are evaluating infection characteristics of the eye in an *in vivo* model.

Discussion

Previously, we reported the expression of ACE2 and TMPRSS2 among other SARS-CoV-2-associated human genes in tissues of the adult human eye [7]. Here, we demonstrate human ocular surface cells become infected when exposed to SARS-CoV-2. Our data show that when compared to other cell types of the eye, the ocular surface ectoderm expresses the receptors used by SARS-CoV-2 to infect human cells and that these cells become infected when exposed to the virus. Similar to what we previously observed in tissues of the respiratory system[26], the IFN-I and IFN-III response is suppressed upon SARS-CoV-2 infection. In addition to these main observations, we show the ocular surface ectoderm derived from zone 3 of the hESC-derived SEAM organoids is a useful model for studying SARS-CoV-2 infection. These cells not only express the typical markers of ocular surface ectoderm, but sub-clusters can be identified with similarity to subtypes of cells from the ocular surface ectoderm such as corneal endothelium, corneal stroma, corneal epithelium, and conjunctiva. In addition, presumptive conjunctiva and proto-corneal cells in the SEAM eye organoids not only express ACE2 and TMPRSS2, but also become infected by SARS-CoV-2. We also reported the expression of another TMPRSS family member, TMPRSS11E, in the same ocular surface ectoderm population expressing ACE2. Interestingly, though IFN-I/-III response was suppressed, an inflammatory response was still mounted – presumably as a result of constitutive NF-kB activation. This latter conclusion is based on the fact that *NFKBIA* is differentially expressed upon SARS-CoV-2 infection. The product of this transcript is responsible for inhibiting the nuclear translocation of p50/p65 but it itself is also transcriptionally induced by these factors – generating a negative feedback loop [27]. The consistent up regulation of *NFKBIA* would suggest that some aspect of SARS-CoV-2 biology results in constitutive NFκB activation.

The success of SARS-CoV-2 infection, like SARS-CoV-1, has been proposed to originate from the inhibition of the normal antiviral immune response and delaying an IFN response. Based on animal models, SARS-CoV-1 was found to induce a robust cytokine response that generally shows a delay in

IFN-I, culminating in the improper recruitment of inflammatory monocyte-macrophage populations [28]. The IFN response did not become active when cells were exposed to SARS-CoV-2, which suggests this IFN suppression is common not only between SARS viruses, but also among human cell types. Whether this suppression is due to dynamics of the angiotensin-renin system is not known. Monocyte-associated and antiviral chemokines CXCL1, CXCL2, CXCL6 were upregulated, although not all reach statistical significance[29-31]. Consistent with previous reports [32,33] as well as description of patients infected with SARS-CoV-2 [34], expression of CXCL1, CXCL2, CXCL3, and CXCL6 suggests neutrophils may also contribute to the disease observed in COVID-19 patients. Monocyte-associated chemokines may predict individuals at risk for developing severe disease symptoms.

While there are few whole transcriptome RNA sequencing reports currently exploring the response of SARS-CoV-2 infection to cells of the eye, non-infected ocular datasets suggest robust inflammatory responses are present. RNA-seq and ATAC-seq of the same samples report open chromatin and transcriptional expression of inflammatory regulators including TNF, IFN-I/-III, and components of NFκB signaling [6]. We observe an elevation in NFκB signaling, while IFN-I/-III biology is suppressed in the network activated by SARS-CoV-2 infection, despite replicating virus. SARS-CoV-2 encodes multiple accessory proteins that are believed to mute the cellular antiviral response by blocking either induction of interferon or perturbating JAK/STAT signaling pathway. The closely related SARS-CoV-1 encodes nsp1 that degrades IFNB mRNA [35] and ORF6 that blocks STAT1 nuclear translocation [36]. Both proteins show high sequence similarity between SARS-CoV-1 and SARS-CoV-2. Also, NFkB signaling can itself selectively suppress IFN responses [37], suggesting there is a tightly controlled orchestration of inflammatory signaling upon SARS-CoV-2 infection.

The evidence of the SARS-CoV-2 infection by the eye in patients with COVID-19 is mixed. While in a controlled environment, conjunctiva of Rhesus monkeys became infected with SARS-CoV-2 [8], the evidence of viral titer in the eye in patients hospitalized for COVID-19 has been less convincing. One meta-analysis study of published reports found that out of 252 patients 11 had positive tear PCR [4]. Another meta-analysis of over 25,000 patients found a significant correlation to eye protection and

reduced rates of infection [38]. Others suggest the risk of becoming infected through the eye is overblown [39]. Whether SARS-CoV-2 may infect the eye directly or from systemic infection via oral or nasal routes is not known. Our data shows the surface ocular cells possess the necessary machinery (ACE2 and TMPRSS2) and become readily infected upon viral exposure from a relatively low (1.0) MOI.

In conclusion, the data presented shows cells of the human ocular surface are at risk for infection by SARS-CoV-2 and thus is an entry vector warranting protection. The limbus seems to be the most at risk, due to the high expression of ACE2 and TMPRSS2, as well as a higher infection titer of any other ocular cell type. The SEAM eye organoid is an effective model by which compounds can be tested to identify prophylactics that may protect the eyes from infection. SARS-CoV-2 effectively suppresses the IFNβ response in cells of the eye, which is consistent with its effect in other tissues of the body. Future studies are warranted to better understand how infection in the eye may lead to transmission into other regions of the body.

Figure Legends

Figure 1. Zone 3 in the SEAM eye organoids composed of cells expressing ocular surface ectoderm gene profile. (A) hESC-derived SEAM organoids were differentiated for 55 days, then processed for single cell RNA-seq and immunohistochemical analysis (n =1 biological replicate). B) Unbiased clustering was conducted using the Seurat Package in R. C) SEAM eye organoids were evaluated for the presence of ocular surface ectoderm markers in Zone 3. D) Cells possessing ocular surface ectoderm annotation were further clustered, presented as UMAP and PCA. E) UMAP presentation of relative expression of known corneal markers across the ocular surface ectoderm cell clusters. F) Heatmap of genes distinguishing each cluster by relative expression. G) Violin plots of known markers of corneal, limbal and conjunctival cells.

Figure 2. Presumptive corneal cell clusters from SEAM eye organoids express ACE2 and TMPRSS2. A) Relative expression of ACE2 in corneal clusters from SEAM eye organoids presented as

UMAP and violin plot. B) ACE2 positive cells evaluated by Jensen TISSUES, Mouse Gene Atlas and Gene Ontology analyses. C) Relative expression of TMPRSS2 in corneal clusters from SEAM eye organoids presented as UMAP and violin plot. D) TMPRSS2 positive cells evaluated by Jensen TISSUES, Mouse Gene Atlas and Gene Ontology analyses. E) Table showing total cell number and percentage of the corneal cells from SEAM eye organoids expressing potential SARS-CoV-2 targets. F) Violin plots of cell clusters and their respective relative expression of genes central to corneal function as well as inflammatory responses to viral entry.

Figure 3. SARS-CoV-2 induces an inflammatory response in infected human adult corneal tissues and hESC-derived SEAM corneal cells. A) Adult human corneal cells isolated from two genetically different adult human donor eyes were infected with SARS-CoV-2, then sequenced for the presence of viral genome transcripts and mapped (n=2 biological replicates). B) RNA-sequencing analysis comparison between non-infected controls and infected cells uncovers the upregulation of an inflammatory network. The five most up regulated genes are labeled by name. Vertical lines indicate a log2 fold change of +/- 0.5 and the horizontal line indicates an adjusted p-value = 0.05. C) Gene network analysis of upregulated genes from (B) identifies an inflammatory complex and a complex involved in mitosis. D) hESC-derived SEAM eye organoids were infected with SARS-CoV-2, then sequenced for presence of viral genome transcripts and mapped (n = 1 biological replicate). E) Table of reads per million (RPM) of genes associated with SARS-CoV-2 infection.

Figure 4. Ocular cell types isolated from adult human eyes infected with SARS-CoV-2. A selection of ocular tissues (cornea (n=4), limbus (n=3), sclera (n =4), iris (n=3), RPE (n=2), choroid (=3) biological replicates) were isolated from adult human cadaver donor eyes and cultured. Cells were exposed to 0.1units/cell of active SARS-CoV-2 virus for 48 hrs. A) Immunofluorescence imaging of ocular cells upon staining for active SARS-CoV-2 virus and ACE-2 receptor expression. B) RNA was isolated and qPCR analysis was conducted to evaluate expression of SARS-CoV-2, C) ACE-2 and D)

TMPRSS2 relative to internal controls. Y-axis scaled in log^{10} format. Scale bars = 100μm. Error bar indicates SEM.

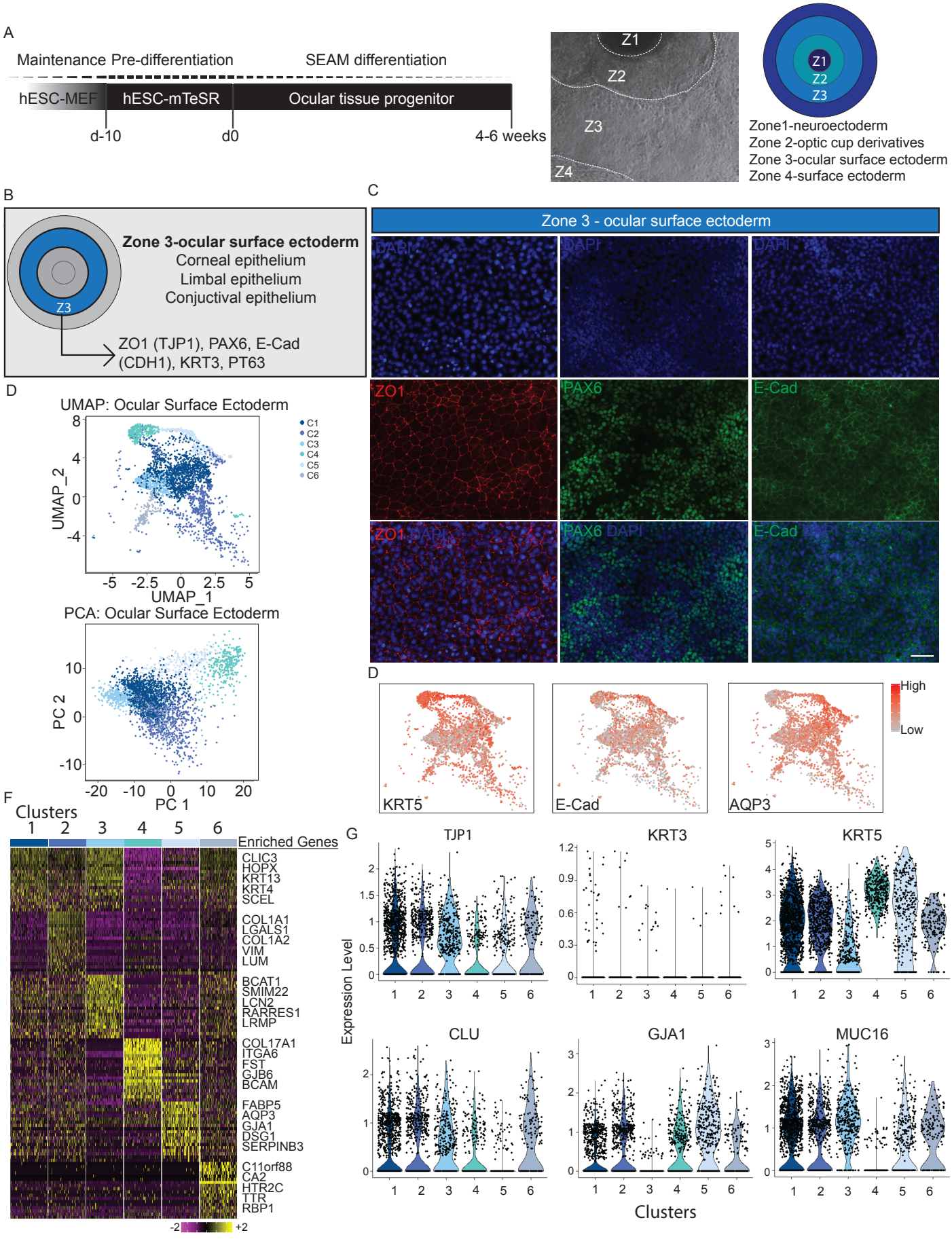

330 Figure 2

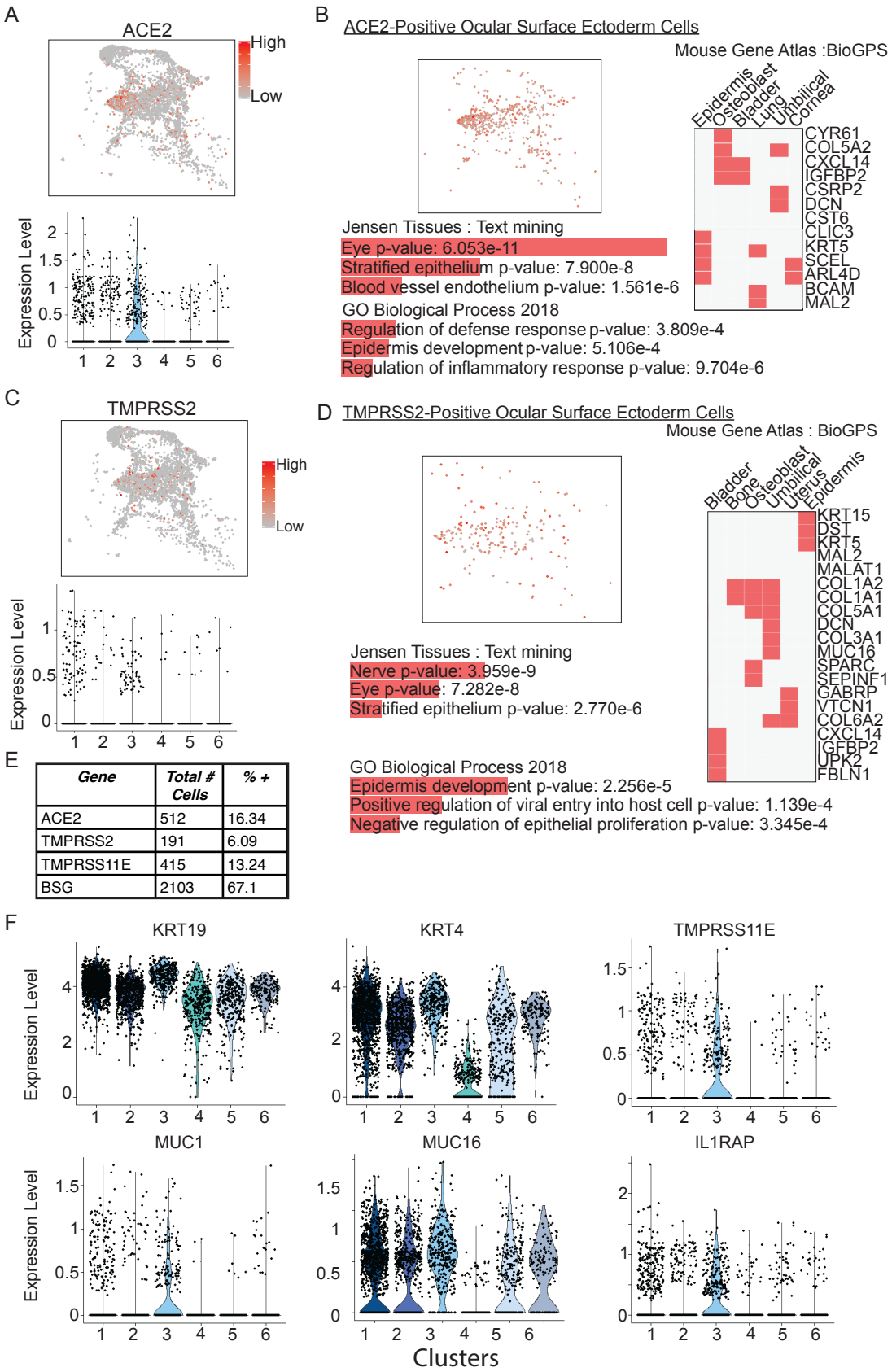

Gene	*Total # Cells*	*% +*
ACE2	512	16.34
TMPRSS2	191	6.09
TMPRSS11E	415	13.24
BSG	2103	67.1

331

332

333

334 Figure 3

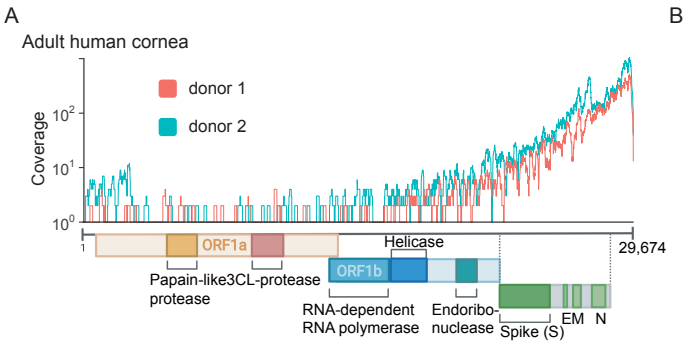

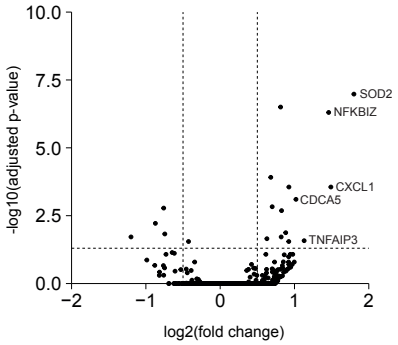

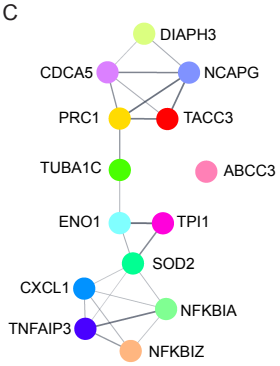

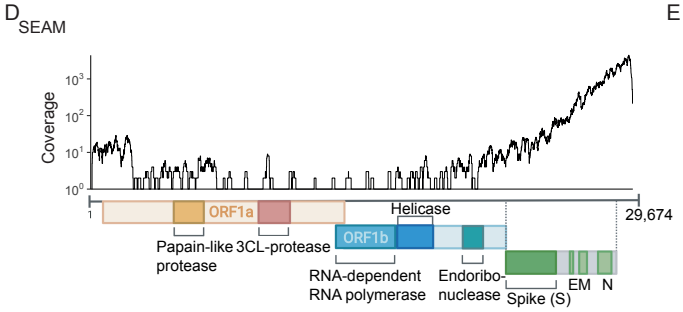

E

Gene	*RPM*
ACE2	30.5
TMPRSS2	16.3
BSG	3399.6
FURIN	100.7
IFNB	0
SARS-CoV-2	*1767.1*

335

336

337 Figure 4

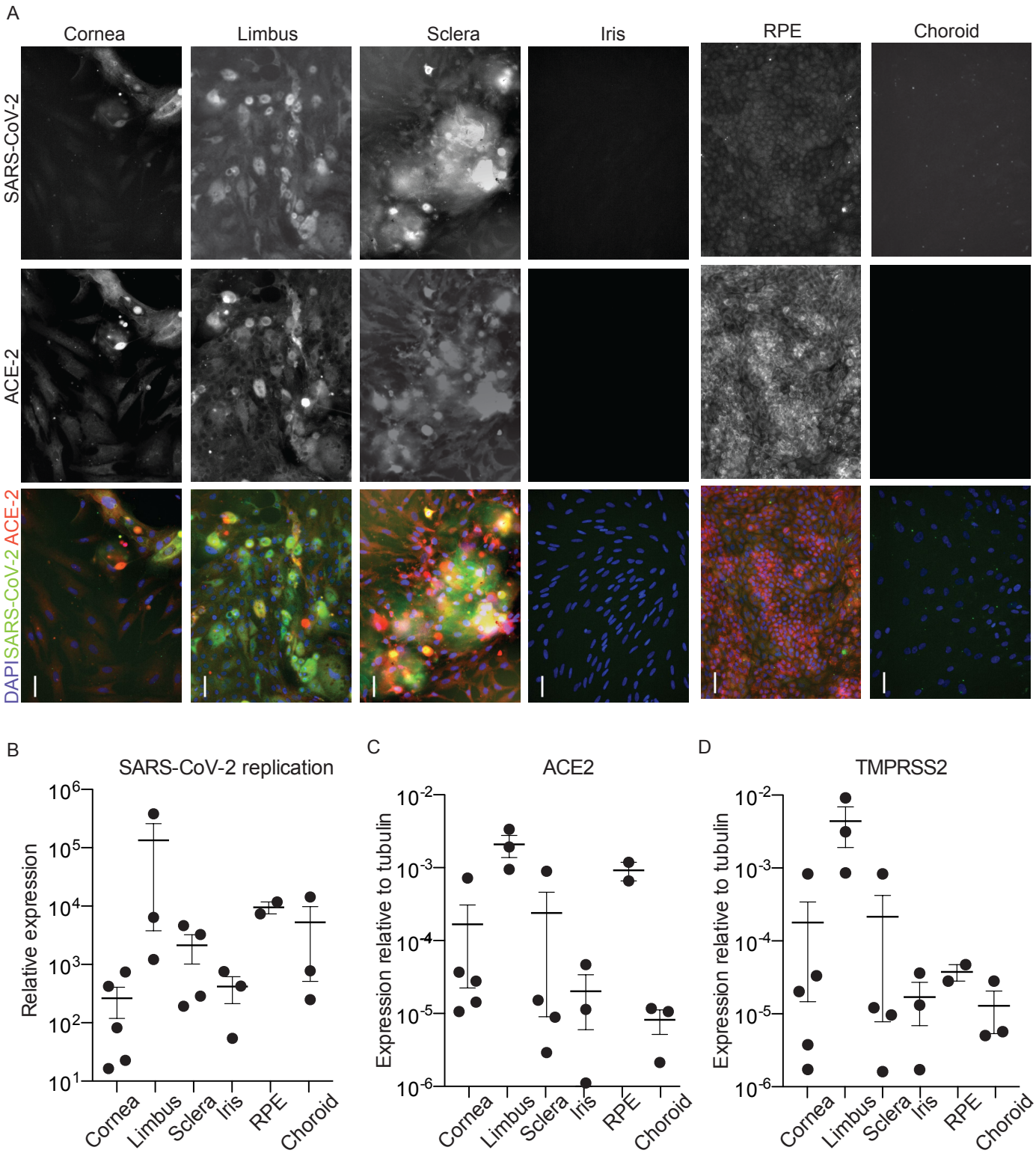

338

339

340

341

Author Contributions

Conceptualization, TAB and BRT; Methodology, BM, AZE, RM, TAB, BRT; Software, TAB and BRT; Investigation, BM, AZE, RM; Resources, TAB; Writing, BM, AZE, RM, BRT; Visualization: BM, AZE, RM; Supervision, TAB and BRT; Project Administration, TAB and BRT; Funding, TAB and BRT.

Data availability

All raw data is available upon reasonable request. Sequencing data has been deposited on https://www.ncbi.nlm.nih.gov/geo/subs/, accession number GSEXXX.

Acknowledgements

We would like to thank the patients and families who generously donated for the research conducted. We would like to thank the Eye Bank for Sight Restoration, NY, NY for their continual support and hard work at procuring donations. We would like to thank Dr. Barbara Corneo for manuscript review. The National Eye Institute (NEI), Bethesda, MD, USA, extramural grant 1R21EY030215-01 and the Icahn School of Medicine at Mount Sinai supported this study. We would like to thank the Carlsberg Foundation, DK for supporting this work.

Materials and Methods

Adult human eye tissue dissection and dissociation. Human globes from donors aged between 36 and 90 years were obtained within 40 h of death from the Eye-Bank for Sight Restoration, Inc., New York, NY, and Miracles in Sight, Winston-Salem, NC. The eye tissues were separated from the eye globe using forceps and scissors then cut into 1mm^2 pieces and placed into 2% collagenase (Worthington, NJ), 3ug/ml DNase I Solution (STEMCELL Technologies) and 2uM Thiazovivin ROCK Inhibitor for a minimum of 2 hours. Cells were isolated from the tissue pieces by trituration, then pelleted by centrifugation at 356 x g for 5 mins and plated into tissue culture treated plates coated with Synthemax II (Corning, AZ) with Dulbecco's Modified Eagle Medium: Nutrient Mix F-12 (DMEM/F12,

Life Technologies), containing 10% Heat Inactivated Fetal Bovine Serum (FBS, Sigma), and 2 uM Thiazovivin ROCK inhibitor. Cells were frozen down prior to single-cell RNA sequencing using CryoStor CS2 Freeze Media in Mr. Frosty containers.

Immunofluorescence staining. Cells were fixed with 4% paraformaldehyde (PFA, Fisher) for 24 h, rinsed 3 times with phosphate buffered saline (PBS), and incubated with 0.03% Triton X-100 (Fisher), 1% bovine serum albumin (BSA) and 5% Normal Goat Serum (Jackson ImmunoResearch Laboratories, Inc.) for 1h to permeabilize cells and block non-specific reaction. Primary antibodies (Supplementary Table 1) were resuspended in 1% BSA in PBS and added for overnight incubation at 4 °C. Cells were then rinsed 3 times, and then incubated with the corresponding Alexa Fluor conjugated secondary antibodies and DAPI (Supplementary Table 2) at room temperature for 45 min. Finally, cells were rinsed 3 times and PBS was added. Images were taken using a Leica DMI6000 inverted microscopy.

Single-cell RNA sequencing. Frozen vials of freshly isolated adult human tissues and SEAM ocular cultures collected on day 55 of differentiation were used for single cell RNA-seq. Viability of single cells was assessed using Trypan Blue staining, and debris-free suspensions of >80% viability were deemed suitable for single cell RNA Seq. Cells were processed using the 10X Genomics Chromium controller v3.16 and the Chromium Single Cell 3' Library and Gel Bead Kit v3.0 using an input of ~10,000 cells. Gel beads were prepared according to standard manufacturer's protocols. Oil partitions of a single-cell and oligo coated gel beads (GEMs) were captured and reverse transcription was performed, resulting in cDNA tagged with a cell barcode and unique molecular index (UMI). Next, GEMs were broken, and cDNA was amplified and quantified using Agilent Bioanalyzer High Sensitivity chip (Agilent Technologies) and QuBit analysis (Thermofisher). The samples were sequenced on the Novaseq 6000 Illumina sequencer with S4 flow cell, (100/paired end reads) targeting a depth of 50,000-100,000 reads per cell using v3 chemistry at the genomics core facility at Mount Sinai. Fastq files were generated using Cell Ranger Single-Cell Software Suite (v3.1) and were aligned to the grch38 reference

genome. Downstream analyses and graph visualizations were performed in the Seurat R package (v. 3.1.2). Briefly, we removed cells with unique gene counts greater than 5,500 (potential doublets) and less than 500. After removing the unwanted cells, 3,380 cells from the various adult human tissues and 5,669 cells from the SEAM culture were normalized by a global-scaling normalization method (LogNormalize) with the default scale factor (10,000). Linear dimensional reduction was performed by PCA, and following which clustering was performed. The results were visualized using Uniform Manifold Approximation and Projection (UMAP) plots for dimension reduction. Violin and individual gene UMAP plots were generated using the Seurat R package. Heatmaps were generated from the top 20 differentially expressed genes per cluster, and some were using a subset of 100 cells per cluster, as indicated in the figure legends. Cluster annotation was guided by manual gene expression notation, which was complemented by Enrichr gene set enrichment analysis, using the top 100 differentially expressed genes for each cluster. Jensen TISSUES text mining provided the association between genes and human tissues, the Mouse Gene Atlas from BioGPS was used for cell type specifications and gene ontologies were generated using the GO biological process 2018 terms.

Quantitative real-time PCR analysis Cells were lysed in TRIzol Reagent (Invitrogen) and separated into an aqueous and an organic layer by centrifugation following the addition of chloroform. RNA was precipitated from the aqueous layer with isopropanol, washed in 75% ethanol and resuspended in nuclease free ddH_2O. Prior to reverse transcription, samples were DNase treated with DNA-free DNA removal kit (Invitrogen). cDNA was generated using oligo d(T) primers (Invitrogen) and SuperScript II Reverse Transcriptase (Thermo Fisher). Quantitative real-time PCR was performed on a LightCycler 480 Instrument II (Roche) using KAPA SYBR FAST qPCR Master Mix Kit (Kapa Biosystems) and primers specific for SARS-CoV-2 N subgenomic RNA and *TUBA1A, ACE2, TMPRSS2, IL6* and *IFNB* spanning at least one intron (except IFNB) (Table S1). Delta-delta-cycle threshold (ΔΔCT) was determined relative to mock-infected samples. Viral RNA levels were normalized to *TUBA1A* and depicted as fold change over mock-infected samples.

RNA sequencing of viral infections 1μg of total RNA was enriched for polyadenylated RNA species and prepared for next-generation sequencing using the TruSeq Stranded mRNA Library Prep Kit (Illumina) according to the manufacturer's instructions. Sequencing libraries were sequenced on an Illumina NextSeq 500 platform.

Bioinformatic analyses Raw reads were aligned to the human genome (hg19) using the RNA express app on Basespace (Illumina) and differential gene expression was determined using the DEseq2 protocol [REF: PMID 25516281]. STRING was used to search for enriched biological processes among the differentially expressed genes (log2 fold change > 0.5, adjusted p-value < 0.05). Raw reads were aligned to the SARS-CoV-2 genome (SARS-CoV-2/USA-WA1/2020 isolate, GenBank accession no. MN985325.1) using bowtie2 and read coverage was visualized using ggplot2 in R.

Virus infections Live virus isolate was deposited by the Center for Disease Control and Prevention and obtained through BEI Resources, NIAID, NIH. The strain SARS-CoV-2/USA-WA1/2020 was used for all experiments. Virus stocks were propagated on Vero E6 cells (ATCC, CRL-1586) and serum in the cell media was reduced to 2% for all infection experiments. All experiments that involved live SARS-CoV-2 virus were carried out in a CDC/USDA-approved biosafety-level 3 (BSL-3) facility at the Icahn School of Medicine at Mount Sinai (New York, USA) in accordance with institutional biosafety requirements. All infected samples were inactivated by lysis in TRIzol Reagent (Invitrogen) or 24h incubation in 5% paraformaldehyde prior to removal from the BSL-3 facility.

Human embryonic stem cells culture and maintenance. Human embryonic stem cell (hESC) line H9 was obtained from WiCell. hESCs were cultured and maintained on irradiated MEFs in Dulbecco's Modified Eagle Medium: Nutrient Mix F-12 (DMEM/F12, Life Technologies), containing 20% knockout serum replacement (KSR, Life Technologies) and supplemented with 1X L-Glutamine (Life

Technologies), 1X MEM Non-Essential Amino Acids Solution (Life Technologies), 1X Penicillin-Streptomycin (10,000 U/mL, Life Technologies), 0.1 mM 2-mercaptoethanol (Sigma). 10 ng/ml FGF-basic (Gibco) was freshly added to media before use. Prior to differentiation, hESCs were seeded onto Matrigel-coated dishes (Corning) in mTeSR1 (STEMCELL Technologies) media for at least three passages.

SEAM ocular culture differentiation. The differentiation of hESCs was performed as indicated in Fig.3A. First, hESCs were seeded as single cells onto Matrigel-coated dishes at 500cells cm^{-2} (5,000 cells in one well of a 6 Well plate), after which they were cultured in mTeSR1 media for 10 days to achieve round small-to-medium-sized separate colonies. Half of the culture medium was then changed to SEAM differentiation media; GMEM (Life Technologies), 10% knockout serum replacement (KSR, Life Technologies) and supplemented with 1X L-Glutamine (Life Technologies), 1X MEM Non-Essential Amino Acids Solution (Life Technologies), 1X Penicillin-Streptomycin (10,000 U/mL, Life Technologies), Sodium Pyruvate (100mM, Life Technologies) and 0.1 μM 2-mercaptoethanol (Sigma). Media changes were performed three times per week throughout the differentiation, in which half of the media was changed for the first week of differentiation, after which full media changes were made. After four to seven weeks of differentiation, SEAM structures were mature and pigmented, at which point they were analyzed and/or harvested.

SEAM ocular culture dissociation. Differentiated SEAM cultures were dissociated in the incubator for 1-hour at 37 °C, 20% O_2, 5% CO_2 using 2.5 mg/ml Collagenase 2 (Worthington Biochemical Corporation) in Hanks' Balanced Salt Solution with 3ug/ml DNase I Solution (STEMCELL Technologies) and 2uM Thiazovivin ROCK Inhibitor. The harvested cells were washed with Dulbecco's Modified Eagle Medium: Nutrient Mix F-12 (DMEM/F12, Life Technologies), containing 0.1% BSA, 3μg/ml DNase I Solution and 2 uM Thiazovivin and then filtered with a 40um cell strainer (Corning).

Cells were frozen down prior to single-cell RNA sequencing in 90% Heat Inactivated Fetal Bovine Serum (FBS, Sigma) and 10% DMSO (COMPANY) using Mr. Frosty containers.

475 **KEY RESOURCES TABLE**

REAGENT or RESOURCE	SOURCE	IDENTIFIER
Antibodies		
Mouse-anti-Sars-CoV-2 Spike (S)		2B3E5
Rb pAb to ACE2	Abcam	AB15348 Lot: GR3333640-8
Alexa Fluor 488 F(ab')2 fragment nt of goat anti-mouse IgG	Invitrogen	A11017 Lot: 2108802
Alexa Fluor 647 F(ab')2 fragment nt of goat anti-Rabbit IgG	Invitrogen	A21246 Lot: 2069609
Bacterial and Virus Strains		
SARS-CoV-2 isolate USA-WA1/2020	BEI Resources	Cat# NR-52281
Biological Samples		
Human eye globes	Eye-Bank for Sight Restoration	
Chemicals, Peptides, and Recombinant Proteins		
Collagenase	Worthington	LS004176
Ambion DNase I Solution	Invitrogen	AM2222
Thiazovivin	Stem Cell Technologies	100-0247
Synthemax II	Corning	3535
CryoStor CS2 Freeze Media	Sigma-Aldrich	C3124
TRIzol Reagent	Invitrogen	15596026
Matrigel	Corning	354230
Critical Commercial Assays		
Chromium Single Cell 3' Library and Gel Bead Kit v3.0	10xGenomics	
10X Genomics Chromium controller v3.16	10xGenomics	
DNA-free DNA removal kit	Invitrogen	AM1906
KAPA SYBR FAST qPCR Master Mix Kit Universal	Kapa Biosystems	Cat# KK4601
TruSeq Stranded mRNA Library Prep Kit	Illumina	Cat# 20020594
Deposited Data		
Mouse Gene Atlas	BioGPS	http://biogps.org/downloads/
DEseq2 protocol		PMID 25516281
SARS-CoV-2/USA-WA1/2020 isolate	GenBank	MN985325.1
Experimental Models: Cell Lines		
Human: Passage 35-40 H9 ES cells	WiCell	N/A
Adult human RPE cells, Passage 1-3	This paper	N/A
Adult human Cornea cells, Passage 1-3	This paper	N/A
Adult human Limbus cells, Passage 1-3	This paper	N/A
Adult human choroid cells, Passage 1-3	This paper	N/A
Adult human Iris cells, Passage 1-3	This paper	N/A
Adult human Iris cells, Passage 1-3	This paper	N/A
Oligonucleotides		
Primer: Sars-CoV-2 N sgRNA Forward: CTCTTGTAGATCTGTTCTCTAAACGAAC	(Blanco-Melo et al. 2020)	[40]
Primer: Sars-CoV-2 N sgRNA Reverse: GGTCCACCAAACGTAATGCG	(Blanco-Melo et al. 2020)	[40]
Primer: *TUBA1A* Forward: GCCTGGACCACAAGTTTGAC	(Blanco-Melo et al. 2020)	[40]
Primer: *TUBA1A* Reverse: TGAAATTCTGGGAGCATGAC	(Blanco-Melo et al. 2020)	[40]

Primer: *ACE2* Forward: CGAGTGGCTAATTTGAAACCAAGAA	(Zhang et al. 2020)	41
Primer: *ACE2* Reverse: ATTGATACGGCTCCGGGACA	(Zhang et al. 2020)	41
Primer: *TMPRSS2* Forward: GTCCCCACTGTCTACGAGGT	(Vidal et al. 2015)	42
Primer: *TMPRSS2* Reverse: ATTGATACGGCTCCGGGACA	(Vidal et al. 2015)	42
Primer: *IL6* Forward: GGTCAGAAACCTGTCCACTG	This paper	N/A
Primer: *IL6* Reverse: CAAGAAATGATCTGGCTCTG	This paper	N/A
Primer: *IFNB* Forward: ACAGCATCTGCTGGTTGAAG	(Blanco-Melo et al. 2020)	40
Primer: *IFNB* Reverse: AGGCAAGGCTATGTGATTAC	(Blanco-Melo et al. 2020)	40
Software and Algorithms		
Cell Ranger Single-Cell Software Suite (v3.1)		
Seurat R package	Seurat et al., 2019	43
Jensen TISSUES text	Jensen Lab	https://tissues.jensenlab.org
ImageJ	Schneider et al., 2012	44
bowtie2 R package	Langmead and Salzberg, 2012	45
ggplot2 R package	Wickham H., 2016	https://ggplot2.tidyverse.org. DOI:10.1007/978-0-387-98141-3
RNA-Express v1.1.10	Ilumina	http://basespace.illumina.com/dashboard
STRING	(Szklarczyk et al. 2019)	46
R	R Foundation for Statistical Computing,	https://www.R-project.org/
BaseSpace	Illumina	http://basespace.illumina.com/dashboard

476

477

478

Literature Cited

1 Lai, T. H. T., Tang, E. W. H., Chau, S. K. Y., Fung, K. S. C. & Li, K. K. W. Stepping up infection control measures in ophthalmology during the novel coronavirus outbreak: an experience from Hong Kong. *Graefes Arch Clin Exp Ophthalmol* **258**, 1049-1055, doi:10.1007/s00417-020-04641-8 (2020).

2 Masters, P. S. & Perlman, S. Coronaviridae. *Fields virology* **1**, 825-858 (2013).

3 de Wit, E., van Doremalen, N., Falzarano, D. & Munster, V. J. SARS and MERS: recent insights into emerging coronaviruses. *Nature reviews. Microbiology* **14**, 523-534, doi:10.1038/nrmicro.2016.81 (2016).

4 Aiello, F. *et al.* Coronavirus disease 2019 (SARS-CoV-2) and colonization of ocular tissues and secretions: a systematic review. *Eye (Lond)*, doi:10.1038/s41433-020-0926-9 (2020).

5 Mousavizadeh, L. & Ghasemi, S. Genotype and phenotype of COVID-19: Their roles in pathogenesis. *Journal of microbiology, immunology, and infection = Wei mian yu gan ran za zhi*, doi:10.1016/j.jmii.2020.03.022 (2020).

6 Collin, J. *et al.* Co-expression of SARS-CoV-2 entry genes in the superficial adult human conjunctival, limbal and corneal epithelium suggests an additional route of entry via the ocular surface. *The ocular surface*, doi:10.1016/j.jtos.2020.05.013 (2020).

7 Hamashima, K. *et al.* Potential modes of COVID-19 transmission from human eye revealed by single-cell atlas. *bioRxiv*, 2020.2005.2009.085613, doi:10.1101/2020.05.09.085613 (2020).

8 Deng, W. *et al.* Ocular conjunctival inoculation of SARS-CoV-2 can cause mild COVID-19 in Rhesus macaques. *bioRxiv*, 2020.2003.2013.990036, doi:10.1101/2020.03.13.990036 (2020).

9 Hohdatsu, T., Okada, S., Ishizuka, Y., Yamada, H. & Koyama, H. The prevalence of types I and II feline coronavirus infections in cats. *The Journal of veterinary medical science* **54**, 557-562, doi:10.1292/jvms.54.557 (1992).

10 Robbins, S. G., Detrick, B. & Hooks, J. J. Retinopathy following intravitreal injection of mice with MHV strain JHM. *Adv Exp Med Biol* **276**, 519-524, doi:10.1007/978-1-4684-5823-7_72 (1990).

11 Nakagaki, K., Nakagaki, K. & Taguchi, F. Receptor-independent spread of a highly neurotropic murine coronavirus JHMV strain from initially infected microglial cells in mixed neural cultures. *Journal of virology* **79**, 6102-6110, doi:10.1128/JVI.79.10.6102-6110.2005 (2005).

12 Hayashi, R. *et al.* Co-ordinated ocular development from human iPS cells and recovery of corneal function. *Nature* **531**, 376-380, doi:10.1038/nature17000 (2016).

13 Kasper, M., Moll, R., Stosiek, P. & Karsten, U. Patterns of cytokeratin and vimentin expression in the human eye. *Histochemistry* **89**, 369-377, doi:10.1007/BF00500639 (1988).

14 Verkman, A. S., Ruiz-Ederra, J. & Levin, M. H. Functions of aquaporins in the eye. *Prog Retin Eye Res* **27**, 420-433, doi:10.1016/j.preteyeres.2008.04.001 (2008).

15 Merjava, S., Neuwirth, A., Tanzerova, M. & Jirsova, K. The spectrum of cytokeratins expressed in the adult human cornea, limbus and perilimbal conjunctiva. *Histology and histopathology* **26**, 323-331, doi:10.14670/HH-26.323 (2011).

16 Matsuyama, S. *et al.* Efficient activation of the severe acute respiratory syndrome coronavirus spike protein by the transmembrane protease TMPRSS2. *Journal of virology* **84**, 12658-12664, doi:10.1128/JVI.01542-10 (2010).

17 Joseph, J., Knobler, R. L., Lublin, F. D. & Burns, F. R. Regulation of the expression of intercellular adhesion molecule-1 (ICAM-1) and the putative adhesion molecule Basigin on murine cerebral endothelial cells by MHV-4 (JHM). *Adv Exp Med Biol* **342**, 389-391, doi:10.1007/978-1-4615-2996-5_60 (1993).

18 Ulrich, H. & Pillat, M. M. CD147 as a Target for COVID-19 Treatment: Suggested Effects of Azithromycin and Stem Cell Engagement. *Stem cell reviews and reports* **16**, 434-440, doi:10.1007/s12015-020-09976-7 (2020).

19 Zmora, P. *et al.* DESC1 and MSPL activate influenza A viruses and emerging coronaviruses for host cell entry. *Journal of virology* **88**, 12087-12097, doi:10.1128/JVI.01427-14 (2014).

20 Yamaya, M. *et al.* The serine protease inhibitor camostat inhibits influenza virus replication and cytokine production in primary cultures of human tracheal epithelial cells. *Pulmonary pharmacology & therapeutics* **33**, 66-74, doi:10.1016/j.pupt.2015.07.001 (2015).

21 Kyrieleis, O. J. *et al.* Crystal structure of the catalytic domain of DESC1, a new member of the type II transmembrane serine proteinase family. *The FEBS journal* **274**, 2148-2160, doi:10.1111/j.1742-4658.2007.05756.x (2007).

22 Bonnin, A., Danneels, A., Dubuisson, J., Goffard, A. & Belouzard, S. HCoV-229E spike protein fusion activation by trypsin-like serine proteases is mediated by proteolytic processing in the S2' region. *The Journal of general virology* **99**, 908-912, doi:10.1099/jgv.0.001074 (2018).

23 Lai, M. M., Patton, C. D. & Stohlman, S. A. Further characterization of mRNA's of mouse hepatitis virus: presence of common 5'-end nucleotides. *Journal of virology* **41**, 557-565 (1982).

24 Wu, H. Y. & Brian, D. A. Subgenomic messenger RNA amplification in coronaviruses. *Proc Natl Acad Sci U S A* **107**, 12257-12262, doi:10.1073/pnas.1000378107 (2010).

25 Coutard, B. *et al.* The spike glycoprotein of the new coronavirus 2019-nCoV contains a furin-like cleavage site absent in CoV of the same clade. *Antiviral research* **176**, 104742, doi:10.1016/j.antiviral.2020.104742 (2020).

26 Daniel Blanco-Melo, B. E. N.-P., Wen-Chun Liu, Skyler Uhl, Daisy Hoagland, Rasmus Møller, Tristan X. Jordan, Kohei Oishi, Maryline Panis, David Sachs, Taia T. Wang, Robert E. Schwartz, Jean K. Lim, Randy A. Albrecht, Benjamin R. tenOever. Imbalanced host response to SARS-CoV-2 drives development of COVID-19. *Cell* **Preprint** (2020).

27 Mitchell, S., Vargas, J. & Hoffmann, A. Signaling via the NFkappaB system. *Wiley interdisciplinary reviews. Systems biology and medicine* **8**, 227-241, doi:10.1002/wsbm.1331 (2016).

28 Channappanavar, R. *et al.* Dysregulated Type I Interferon and Inflammatory Monocyte-Macrophage Responses Cause Lethal Pneumonia in SARS-CoV-Infected Mice. *Cell host & microbe* **19**, 181-193, doi:10.1016/j.chom.2016.01.007 (2016).

29 Bizzarri, C. *et al.* Single-cell analysis of macrophage chemotactic protein-1-regulated cytosolic Ca2+ increase in human adherent monocytes. *Blood* **86**, 2388-2394 (1995).

30 Loetscher, P., Seitz, M., Clark-Lewis, I., Baggiolini, M. & Moser, B. Monocyte chemotactic proteins MCP-1, MCP-2, and MCP-3 are major attractants for human CD4+ and CD8+ T lymphocytes. *FASEB J* **8**, 1055-1060, doi:10.1096/fasebj.8.13.7926371 (1994).

31 Eugenin, E. A. *et al.* CCL2/monocyte chemoattractant protein-1 mediates enhanced transmigration of human immunodeficiency virus (HIV)-infected leukocytes across the blood-brain barrier: a potential mechanism of HIV-CNS invasion and NeuroAIDS. *J Neurosci* **26**, 1098-1106, doi:10.1523/JNEUROSCI.3863-05.2006 (2006).

32 McLoughlin, R. M. *et al.* Differential regulation of neutrophil-activating chemokines by IL-6 and its soluble receptor isoforms. *J Immunol* **172**, 5676-5683, doi:10.4049/jimmunol.172.9.5676 (2004).

33 Schenk, B. I., Petersen, F., Flad, H. D. & Brandt, E. Platelet-derived chemokines CXC chemokine ligand (CXCL)7, connective tissue-activating peptide III, and CXCL4 differentially affect and cross-regulate neutrophil adhesion and transendothelial migration. *J Immunol* **169**, 2602-2610, doi:10.4049/jimmunol.169.5.2602 (2002).

34 Chen, N. *et al.* Epidemiological and clinical characteristics of 99 cases of 2019 novel coronavirus pneumonia in Wuhan, China: a descriptive study. *Lancet* **395**, 507-513, doi:10.1016/S0140-6736(20)30211-7 (2020).

35 Narayanan, K. *et al.* Severe acute respiratory syndrome coronavirus nsp1 suppresses host gene expression, including that of type I interferon, in infected cells. *Journal of virology* **82**, 4471-4479, doi:10.1128/JVI.02472-07 (2008).

36 Frieman, M. *et al.* Severe acute respiratory syndrome coronavirus ORF6 antagonizes STAT1 function by sequestering nuclear import factors on the rough endoplasmic reticulum/Golgi membrane. *Journal of virology* **81**, 9812-9824, doi:10.1128/JVI.01012-07 (2007).

37 Cheng, C. S. *et al.* The specificity of innate immune responses is enforced by repression of interferon response elements by NF-kappaB p50. *Science signaling* **4**, ra11, doi:10.1126/scisignal.2001501 (2011).

38 Chu, D. K. *et al.* Physical distancing, face masks, and eye protection to prevent person-to-person transmission of SARS-CoV-2 and COVID-19: a systematic review and meta-analysis. *Lancet*, doi:10.1016/S0140-6736(20)31142-9 (2020).

39 Zhou, Y., Zeng, Y., Tong, Y. & Chen, C. Ophthalmologic evidence against the interpersonal transmission of 2019 novel coronavirus through conjunctiva. *medRxiv*, 2020.2002.2011.20021956, doi:10.1101/2020.02.11.20021956 (2020).

40 Blanco-Melo, D. *et al.* Imbalanced Host Response to SARS-CoV-2 Drives Development of COVID-19. *Cell* **181**, 1036-1045 e1039, doi:10.1016/j.cell.2020.04.026 (2020).

41 Zhang, Q. *et al.* ACE2 inhibits breast cancer angiogenesis via suppressing the VEGFa/VEGFR2/ERK pathway. *Journal of experimental & clinical cancer research : CR* **38**, 173, doi:10.1186/s13046-019-1156-5 (2019).

42 Vidal, S. J. *et al.* A targetable GATA2-IGF2 axis confers aggressiveness in lethal prostate cancer. *Cancer cell* **27**, 223-239, doi:10.1016/j.ccell.2014.11.013 (2015).

43 Stuart, T. *et al.* Comprehensive Integration of Single-Cell Data. *Cell* **177**, 1888-1902 e1821, doi:10.1016/j.cell.2019.05.031 (2019).

44 Schneider, C. A., Rasband, W. S. & Eliceiri, K. W. NIH Image to ImageJ: 25 years of image analysis. *Nat Methods* **9**, 671-675, doi:10.1038/nmeth.2089 (2012).

45 Langmead, B. & Salzberg, S. L. Fast gapped-read alignment with Bowtie 2. *Nat Methods* **9**, 357-359, doi:10.1038/nmeth.1923 (2012).

46 Szklarczyk, D. *et al.* STRING v11: protein-protein association networks with increased coverage, supporting functional discovery in genome-wide experimental datasets. *Nucleic Acids Res* **47**, D607-D613, doi:10.1093/nar/gky1131 (2019).

607 **Supplemental Material Makovoz et al.**

608

609 **Supplemental Figure 1**

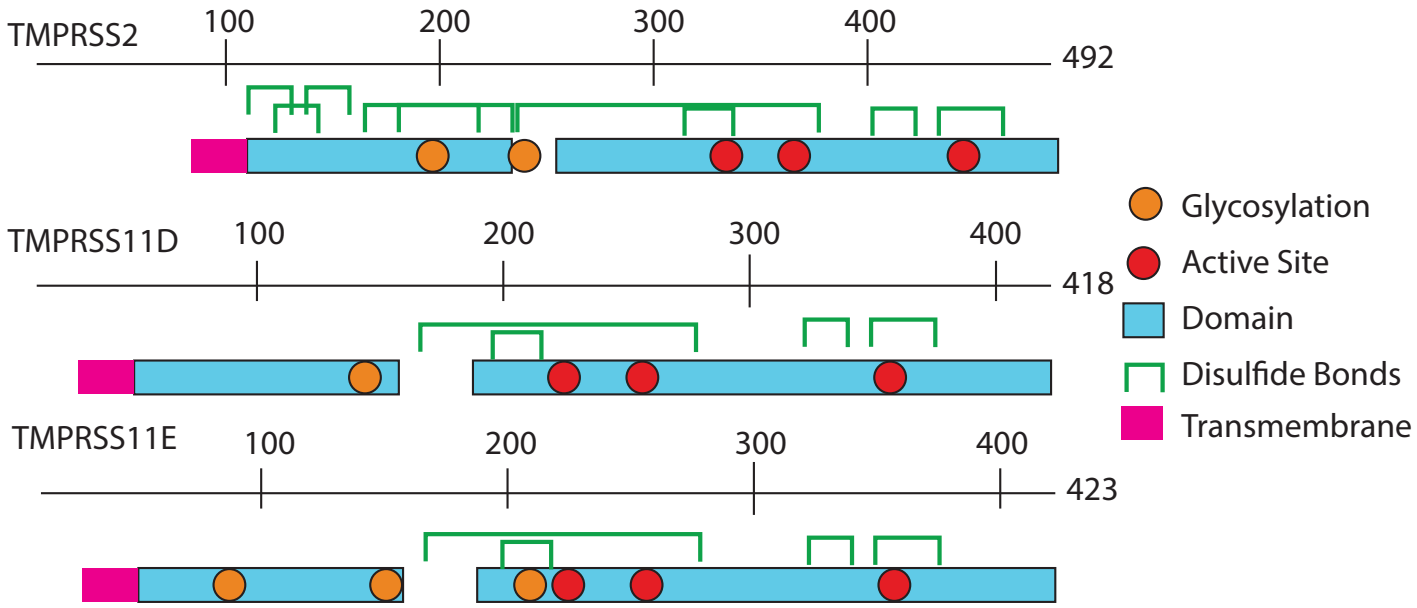

Supplemental Figure 1. Domain alignment of members of the TMPRSS family. Alignment generated with the help of information from Uniprot.org. Active site = protease activity.

610

611

Supplemental Figure 2

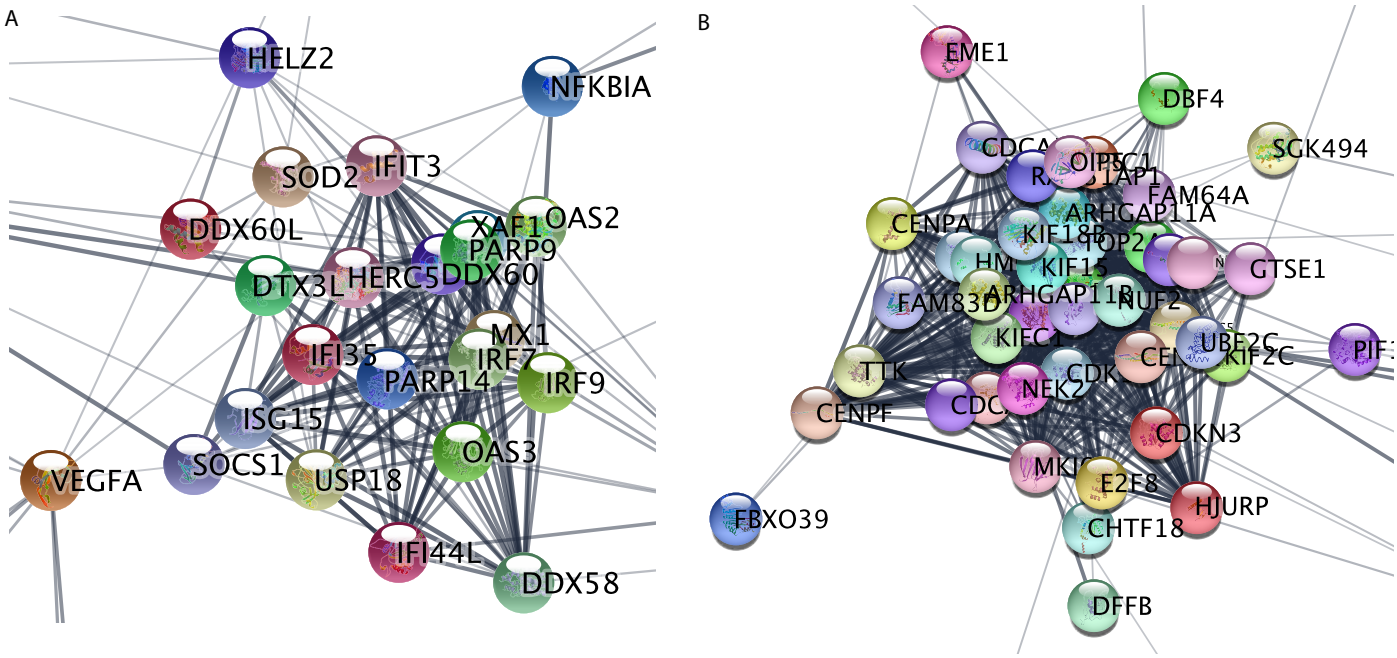

Supplemental Figure 2. Greater networks of differentially expressed genes in corneal cells upon SARS-CoV-2 infection. A) Network of inflammation associated genes. B) Network of cell cycle associated genes.

Supplemental Figure 3

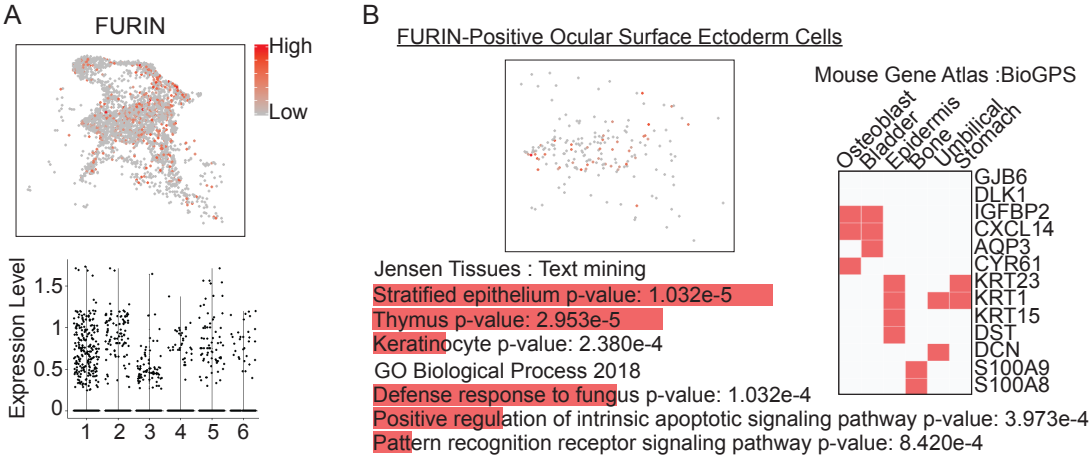

Supplemental Figure 3. Presumptive corneal cell clusters from SEAM eye organoids were evaluated for expression of FURIN. A) Relative expression of FURIN in corneal clusters from SEAM eye organoids presented as UMAP and violin plot. B) FURIN positive cells evaluated by Jensen TISSUES, Mouse Gene Atlas and Gene Ontology analyses.